Mesyl Phosphoramidate Oligonucleotides as Potential Splice Switching Agents: Impact of Backbone Structure on Activity and Intracellular Localization

Suzan M. Hammond[1,#], Olga V. Sergeeva[2,#], Pavel A. Melnikov[3], Larissa Goli[1], Jessica Stoodley[1], Timofei S. Zatsepin[2,4], Dmitry A. Stetsenko[5,6,*], and Matthew J.A. Wood[1]

[1] University of Oxford, Oxford OX3 9DU, UK

[2] Skolkovo Institute of Science and Technology, Moscow 121205, Russia

[3] Serbsky National Medical Research Center for Psychiatry and Narcology, Moscow119034, Russia

[4] Lomonosov Moscow State University, Moscow 119992, Russia

[5] Novosibirsk State University, Novosibirsk 630090, Russia

[6] Institute of Cytology and Genetics, Siberian Branch of the Russian Academy of Sciences, Novosibirsk 630090, Russia

[#] These authors made equal contributions to this work.

* Corresponding author: Dmitry A. Stetsenko, tel.: +7 (383) 363 49 63 , email: d.stetsenko@nsu.ru

RUNNING TITLE

Mesyl Phosphoramidates as Splice Switching Agents

ABSTRACT

A series of 2'-deoxy and novel 2'-*O*-methyl and 2'-*O*-(2-methoxyethyl) (2'-MOE) oligonucleotides with internucleotide methanesulfonyl (mesyl, μ) or 1-butanesulfonyl (busyl, β) phosphoramidate groups have been synthesized for evaluation as potential splice-switching oligonucleotides. Evaluation of their splice-switching activity in spinal muscular atrophy (SMA) patient derived fibroblasts revealed no significant difference in splice-switching efficacy between 2'-MOE mesyl oligonucleotide and the corresponding phosphorothioate (nusinersen). Yet, a survival study with model neonatal mice have shown the antisense 2'-MOE mesyl oligonucleotide to be inferior to nusinersen at the highest dose of 40 mg/kg. A reason for their lower activity *in vivo* as ascertained by cellular uptake study via fluorescent confocal microscopy in HEK293 cell line could possibly be ascribed to compromised endosomal release and/or nuclear uptake of the 2'-OMe or 2'-MOE μ- and β-oligonucleotides as compared to their phosphorothioate analog.

INTRODUCTION

Antisense oligonucleotides have been extensively reviewed in the literature as therapeutic agents that target biologically important RNAs via either RNase H mediated enzymatic cleavage [1-3] or steric modulation of RNA metabolism [4, 5]. While the former type is applicable to a wider range of potential targets including genetic diseases [6], cancers [7], viral [8] and bacterial [9] pathogens, where the target RNA can be destroyed, the latter type works when subtler changes in the RNA activity are required such as splice redirection involving exon skipping or inclusion [10, 11]. A primary therapeutic target in the latter case are monogenic genetic diseases such as Duchenne muscular dystrophy (DMD) [12] and spinal muscular atrophy (SMA) [13]. Up to date, several steric blocking antisense splice-switching oligonucleotides have been approved by FDA for clinical use such as eteplirsen (Exondys 51) [14], golodirsen (Vyondys 53) [15], and nusinersen (Spinraza) [16]. Amongst these, nusinersen has received public recognition as a ‘life-saving drug’ to treat SMA.

Spinal muscular atrophy (SMA) is a leading genetic cause of infant mortality primarily due to motor neuron degeneration and progressive muscle weakness [17]. It results from loss of the ubiquitous survival motor neuron 1 gene, *SMN1* [17, 18]. Human genome contains a second nearly identical copy, *SMN2*, which differs from *SMN1* by a crucial nucleotide transition within exon 7 leading to the predominant generation of an alternative exon 7-excluded mRNA transcript and only marginally functional protein [19-23]. *SMN2* therefore fails to compensate for loss of *SMN1*

unless sufficient copies are present to generate functional levels of full-length SMN protein [18].

A therapeutic approach for SMA utilizes single-stranded antisense splice-switching oligonucleotides to promote inclusion of exon 7 into SMN2 pre-mRNA via steric blocking of pre-mRNA elements pertinent to splice regulation [24]. The clinically approved antisense oligonucleotide against SMA, nusinersen (Spinraza), is an 18-mer oligo-2'-*O*-(2-methoxyethyl) (2'-MOE) ribonucleotide (Fig. 1, **1**) that targets the intron splice silencer N1 (ISS-N1) site within intron 7 [25, 26]. Nusinersen improves survival and motor function in the majority of SMA patients, most prominently in those treated early in disease progression [27]. The drug is administered via intrathecal injection, which to-date appears to be reasonably safe and tolerable in both adult and children patients, even those with spinal problems [28, 29].

The backbone of nusinersen is the phosphorothioate: a phosphate linkage isostere, which is present in a majority of antisense oligonucleotides studied so far [30]. Phosphorothioate groups (PS) increase enzymatic stability and propensity for protein binding that improve cellular uptake, biodistribution and pharmacokinetic properties of the oligonucleotides (PS ONs) [31, 32]. However, adverse effects of PS ONs were also documented, most notably, *in vivo* toxicity, particularly liver damage [33, 34] and complement activation [35, 36]. The concerns over clinical safety of PS ONs have resulted in the repeated refusals of EMA to approve mipomersen (Kynamro), an FDA-approved drug to treat homozygous familial hypercholesterolemia [37], and failure of several PS-modified drug candidates to

make through different phases of clinical trials [38, 39]. Although it was recently reported that a pinpoint sugar modification improved the therapeutic index of RNase H-competent PS ONs [40], the adverse effects associated with the use of phosphorothioate group for antisense ONs remain a serious concern, especially for splice-switching applications, where the need for a life-long treatment was postulated [41]. This highlights the importance of devising new chemistries for antisense oligonucleotide backbone modification.

Recently, we have shown that mesyl (methanesulfonyl) phosphoramidate group (μ) can be an efficient alternative to phosphorothioate (PS) group in antisense oligonucleotides targeting miRNAs [42]. The corresponding RNase H-competent mesyl phosphoramidate oligodeoxynucleotides (μ-ODNs) (Fig. 1, **2a**) were demonstrated to possess increased specificity, reduced toxicity and improved activity over their PS analogues [42]. The results encouraged us to attempt the design of novel steric blocking oligonucleotides incorporating mesyl phosphoramidate (μ) or their extended chain analogue 1-butanesulfonyl (busyl) phosphoramidate (β) groups [43] as potential splice-switching agents by replacing 2'-deoxynucleosides in the backbone with 2'-*O*-methylribonucleosides (Fig. 1, **2b**) or 2'-*O*-(2-methoxyethyl)ribonucleosides (Fig. 1, **2c**). Such sugar modifications are known to increase stability of antisense oligonucleotide duplexes with RNA and completely abolish RNase H activation [44], which is essential for splice-switching applications. We would like to present herein our studies on the cellular uptake and intracellular localization of 2'-MOE mesyl phosphoramidate oligonucleotides (MOE μ-ONs) and

a range of 2'-substituted mesyl and busyl analogs, and evaluation of their splice-switching activity in SMA patient derived fibroblasts and *in vivo* in a neonatal mouse model of SMA.

MATERIALS AND METHODS

Oligonucleotide synthesis

Mesyl (μ) and busyl (β) phosphoramidate oligonucleotides (Table 1) were assembled by automated solid-phase phosphoramidite synthesis replacing aqueous iodine oxidation by Staudinger reaction with either methanesulfonyl azide or 1-butanesulfonyl azide (0.5 M in acetonitrile, 40 min at ambient temperature) in each cycle of chain elongation [43, 45]. After the completion of the synthesis, the oligonucleotides were cleaved from the polymer support and deprotected by standard ammonia treatment followed by consecutive PAGE and RP-HPLC purification as described previously [46]. For confocal microscopy studies, 3'-alkynylated mesyl and busyl phosphoramidate oligonucleotides were labeled with Cy5 azide using Cu(I)-catalyzed 1,3-dipolar alkyne-azide cycloaddition reaction (CuAAC) [46]. As PS oligonucleotides have been reported to undergo significant desulfurization under Cu(I)-mediated click reaction [47], *N*-hydroxysuccinimidyl (NHS) ester of Cy5 dye has been used for acylation of 3'-aminoalkylated oligonucleotide in the latter case. Molecular masses of the oligonucleotides were verified by ESI LC-MS (Table 1).

In vitro evaluation of splice-switching activity in SMA patient fibroblasts

Oligonucleotides were resuspended in nuclease-free water. Type II SMA patient-derived fibroblasts (GM03813, Coriell Institute for Medical Research) were maintained in standard medium (DMEM+GlutaMax (ThermoFischer Scientific, cat. No. 31966-021), 15% fetal bovine serum (FBS), 1% penicillin-streptomycin). 48h before treatment, fibroblasts were seeded in 6-well plates at the density of 140,000 ¢/well.

Lipofectamine 3000 (Invitrogen, cat. No. L3000-001) assisted transfection experiments were performed in 15% FBS, according to the manufacturers' manual. All conditions were conducted in technical triplicates.

After 24 h or 72 h post-treatment, cells were washed with PBS, and cell pellets were collected after trypsinisation and centrifugation (500g, 5 min, 4°C).

RNA was extracted using the Promega Maxwell® RSC simply RNA Cells kit (Promega, cat. No. AS1390), and eluted in 35 µL nuclease-free water. RNA concentration was measured using a UV-Vis spectrophotometer Nanodrop 2000 (ThermoFischer Scientific).

cDNA was prepared from 1 µg RNA, using ABI High Capacity cDNA Reverse Transcription Kits (Applied Biosystems, cat. No. 4368813), following the manufacturers' instructions; and was then diluted to a final concentration of 10 ng/µL.

Quantitative PCR (qPCR) was performed on StepOne™ Real-Time PCR System (Applied Biosystems, ThermoFisher Scientific) using TaqMan™ Fast Advanced

Master Mix, and primers for FL-*SMN* and tot-*SMN* as described in ref [48]. Efficiency of the PCR was corrected for using the LinReg PCR software [49, 50]. Final data was analysed using the method described in ref [51]. Statistical analyses were conducted with Prism v.8, GraphPad Software, which was also used to plot the figures.

Analysis of Cy5-labeled oligonucleotides nuclear uptake by confocal microscopy in fixed HEK293 cells

Solutions of Cy5-labeled ASO (Table 1) in 1× phosphate-buffered saline buffer (PBS) were added to human HEK293 (ATCC CRL-3216) cells in Dulbecco's Modified Eagle Medium Nutrient Mixture F-12 (DMEM/F12) supplemented with 10% FBS, 100 μg/ml streptomycin, 100 U/ml penicillin cultured on poly-L-lysine coated cover glass slides placed to the bottom of a 24-well plate to the final concentration of 1 μM. Cells were cultured at 37°C in humidified air with 5% CO_2 for 24 h. Then glasses with cells were washed with 1×PBS, fixed in 1×PBS containing 4% formaldehyde at room temperature for 20 min, washed with 1×PBS, and permeabilized in 1×PBS with 0.1% Triton X-100 for 5 min. Then glasses were washed twice with 1×PBS for 10 min. Cells were embedded in Mowiol with DAPI (Sigma) prior to imaging. Confocal microscopy was performed using Nikon A1+MP confocal imaging system using a Plan Apo 20x/0,75 Dic N objective (numerical aperture 0.75; Nikon Japan), Apo LWD 40x/1,15 S water immersion objective (numerical aperture 0.15; Nikon, Japan) and Apo tirf 60x/1,49 DIC Oil immersion

objective (numerical aperture 0.49; Nikon, Japan). Images were scanned sequentially using 561 nm diode lasers in combination with a DM561 nm dichroic beam splitter. To describe the nuclear membrane contour, each Z-stack was processed by the intensity threshold of the blue channel (cell nucleus) in the first stage of calculations. Thresholding was performed by the following parameters: area, roundness, intensity of fluorescence. Next, the binary layer of nuclei was subtracted from the binary layer of the sample, allowing to detect fluorescence intensity of the ASO inside the nuclei only.

Live HEK293 cell imaging of Cy5-labeled oligonucleotides internalization by confocal microscopy

1×10^5 HEK293 (ATCC CRL-3216) cells in DMEM/F12 supplemented with 10% FBS, 100 ug/ml streptomycin, 100 U/ml penicillin cultured in the confocal dishes 24 h up to achieving 70% confluence. LysoTracker red DND-99 (Invitrogen) was added to the cells to final concentration of 50 nM and incubated for 10 min. Then cells were washed 3 times with 1×PBS, and the fresh DMEM/F12 medium was added. ASOs (Table 1) in 1×PBS were added to the cells to final concentration of 0.1 mM and incubated for 60 min. The cells were washed 3 times with 1×PBS, and the fresh DMEM/F12 medium was added. Live cell imaging of ASO internalization was carried out at 37°C in humidified air with 5% CO_2 on a Nikon A1+MP confocal imaging system using a Plan Apo 20x/0,75 Dic N objective (numerical aperture 0.75, Nikon, Japan), Apo LWD 40x/1,15 S water immersion objective (numerical aperture

1.15, Nikon, Japan). Images were scanned sequentially using 561 nm and 647 nm diode lasers in combination with a DM405/488/561/633 nm dichroic beam splitter. Differential Interference Contrast Imaging (DIC) microscopy was used to visualize cell contours. The images were analyzed with NIS-elements AR (Nikon Japan). PCC (Pearson's correlation coefficient) and MOC (Manders' overlap coefficient) were used to assess the co-localization rate.

Animal model and dosing

Animal studies were carried out in the Biomedical Sciences Unit, University of Oxford according to procedures authorised and approved by the University of Oxford ethics committee and UK Home Office (project license PDFEDC6F0). SMA-like mouse strain FVB.Cg-Smn1tm1HungTg(SMN2)2Hung/J was generated and maintained as previously described [52, 53]. 2’-MOE oligonucleotides 5'-TCA CTT TCA TAA TGC TGG targeting the SMN2 ISSN1 sequence with phosphorothioate or mesyl phosphoramidate internucleotidic linkages (MOE-Nus-s and MOE-Nus-m, respectively) were tested. Subcutaneous administrations were performed by single (PND0) administrations. Doses of 20 μg/g (2.35 nmol/g for MOE-Nus-m or 2.73 nmol/g for MOE-Nus-s), 30 μg/g (3.58 nmol/g for MOE-Nus-m or 4.10 nmol/g for MOE-Nus-s), or 40 μg/g (4.70 nmol/g for MOE-Nus-m or 5.47 nmol/g for MOE-Nus-s) of ASOs were diluted in 0.9% saline and given at a volume of 10 μl per gram body weight. Scrambled mesyl and phosphorothioate oligonucleotides MOE-Scr-m and MOE-Scr-s 5'-ACT TTC ACT AAT CGT GGT

and luciferase targeted MOE-Luc-m and MOE-Luc-s 5'-TCG AAG TAC TCA GCG TAA G were used as controls. Treated mice were given mash as food supplementation. Weights were taken daily and overall health assessed. Following the humane endpoint, mice were euthanized according to the approved procedure of rising CO_2.

RESULTS

Design and synthesis of novel mesyl and busyl phosphoramidate oligo-2'-*O*-alkyl ribonucleotides

The synthesis of 2'-*O*-alkyl mesyl (μ) and busyl (β) oligonucleotides (Figure 1, **2**) was accomplished according to our previously reported method of automated solid-phase assembly *via* the phosphoramidite method followed by Staudinger reaction with 0.5 M solution of a sulfonyl azide in acetonitrile instead of aqueous iodine oxidation [43, 45]. The Staudinger reaction between the support-bound phosphite triester formed during the phosphoramidite coupling and methanesulfonyl azide or 1-butanesulfonyl azide, respectively, was carried out for 40 min at ambient temperature. Oligonucleotides containing 5'-dimethoxytrityl group (DMTr) were isolated by reverse-phased (RP) HPLC or, if necessary, purified to homogeneity by denaturing PAGE under the same conditions as phosphodiester or PS ONs followed by RP-HPLC to remove phosphodiester impurities. The molecular masses of the μ- and β-oligonucleotides obtained have been confirmed by ESI LC-MS (Table 1).

In vitro evaluation of splice-switching activity in SMA patient fibroblasts

Splice-switching activity of ASOs *in vitro* has been assessed in SMA patient derived fibroblasts. Due to low ASO uptake in fibroblasts via gymnosis we used lipofectamine transfection agent for cell culture studies. Fibroblasts were treated with 0, 1, 10 and 50 nM SMN2 targeted ASOs with nusinersen sequence (Table 1). The nusinersen ASO sequence acts by binding to the ISSN1 sequence of SMN2

intron 7, masking a splicing suppressor region and thereby enhancing exon 7 included transcripts. Splice switching activity was measured *via* qPCR relating the amount of exon 7 included transcripts (*FLSMN*) to the total number of transcripts (*TotalSMN*). TotalSMN was determined by exons 1 and 2a present in all SMN2 derived transcripts. Regardless of the phosphate modification, 2'-deoxy ASOs were not active in these cells (Figure 2, a) as it may be expected because of the different mechanism of action (RNase H recruitment). Nor did busyl phosphoramidate (β) ASOs (me Nus-bm and MOE-Nus-bm) show activity, possibly hinting at unfavorable intracellular localization of β-ASOs. Active ASOs were the 2'-OMe and 2'-MOE with phosphorothioate (PS) and mesyl phosphoramidate (μ) internucleotidic linkages (MOE-Nus-s, MOE-Nus-m, me Nus-s and me Nus-m, respectively) (Figure 2, b and c). Scrambled ASO sequence with the most active 2'-MOE chemistry was inactive with all phosphate modifications (Figure 2, d). The most active in cell culture compounds, MOE-Nus-m and MOE-Nus-s, were selected for further comparison *in vivo*.

Intracellular distribution and endosomal release of phosphorothioate, mesyl (μ) and busyl (β) phosphoramidate oligonucleotides in live cells

We studied intracellular distribution of Cy5-labelled ASOs in live HEK293 cells after unaided uptake (gymnosis) at 0.1 μM concentration of each ASO in the presence of fluorescent labeled lysosome tracker. Three modified phosphate derivatives, namely, phosphorothioate (PS), mesyl (μ) and busyl (β)

phosphoramidate were compared for three backbones: 2'-deoxy, 2'-OMe and 2'-MOE. Deoxy oligonucleotides with phosphorothioate (dNus-s), mesyl (μ) phosphoramidate (dNus-m) or busyl (β) phosphoramidate (dNus-bm) internucleotidic linkages demonstrated approx. 75% of the endosomal release during the first hour of incubation based on the Pearson's correlation coefficient calculation (Suppl. Fig. S2). Introduction of 2'-OMe modifications into the phosphorothioate oligonucleotide (me Nus-s) decreased the release rate of the ASO from endosomes to ~60%. However, switching to 2'-OMe backbone in μ-ASO (me Nus-m) or β-ASO (me Nus-bm) improved endosomal release (~83% and ~72% respectively), and only 17% and 28% of μ-ASO or β-ASO were found in lysosomes. 2'-*O*-Methoxyethyl phosphorothioate ASO (MOE Nus-s) demonstrated reduced release (~65% only). In the case of 2'-MOE mesyl phosphoramidate (MOE Nus-m) the increase of accumulation of μ-ASO in the lysosomes was up to ~60% (~40% of release of μ-ASO in the cell). At the same time 2'-MOE busyl phosphoramidate (MOE Nus-bm) was released from endosomes up to ~72% under the same conditions (Suppl. Fig. S2). Thus, increased hydrophobicity of the μ-ASO or β-ASO improves endosomal escape only in the case of 2'-*O*-alkyl RNA backbone.

Intranuclear distribution of phosphorothioate, mesyl and busyl phosphoramidate oligonucleotides in fixed cells

We studied intranuclear distribution of Cy5-labeled ASOs in fixed HEK293 cells after unaided uptake (gymnosis) at 1 μM concentration of each ASO and 24 h

exposition (Fig. 4). Confocal micrographs demonstrate that the majority of deoxy phosphorothioate (d-Nus-s) is uniformly distributed across cytoplasm and the nucleus, while some amount is concentrated in perinuclear structures. Switch from phosphorothioate to mesyl phosphoramidate in the deoxy series (d-Nus-m) resulted in ASO accumulation predominantly in the cytosol including perinuclear space. Busyl phosphoramidate (d-Nus-bm) modification also resulted in the predominantly cytosolic accumulation of the ASO. Introduction of 2'-OMe groups into the phosphorothioate oligonucleotide (me-Nus-s) resulted in cytoplasmic localization of ASO in perinuclear structures. At the same time, 2'-OMe mesyl phosphoramidate ASO (me-Nus-m) demonstrated not only cytoplasmic localization but some fluorescence was also observed in the nucleus. Switch to busyl phosphoramidate (me-Nus-bm) shifts the localization of ASO to perinuclear region of cytoplasm with clustering near the nucleus. 2'-MOE modification in conjunction with phosphorothioate backbone (MOE-Nus-s) caused accumulation of ASO in the perinuclear region of the cytosol with some fluorescent signals observed in the cell nucleus. Introduction of 2'-MOE modification into mesyl (MOE-Nus-m) or busyl (MOE-Nus-bm) phosphoramidate oligonucleotides resulted in their distribution to endosomes in the cytosol and clustering in the perinuclear region and nucleus.

Calculation of the fluorescent signal intensity in the cell nucleus (Suppl. Table S4) demonstrated that deoxy phosphorothioate (dNus-s) was taken to the nucleus with the highest efficacy whereas mesyl (μ) and busyl (β) phosphoramidate modifications decreased the efficacy ~7 fold. Introduction of 2'-OMe groups into all types of

backbone modification decreased the nuclear localization by ~3-4 times compared to phosphorothioate oligodeoxynucleotide (dNus-s). 2'-MOE modification demonstrated the most significant impact on the level of the intranuclear localization. 2'-MOE modification in conjunction with phosphorothioate backbone demonstrated the lowest signal in the cell nucleus. Thus, addition of the mesyl and busyl phosphoramidate modifications provides the second modality to influence on the intracellular distribution of 2'-*O*-alkyl oligonucleotides.

Systemic administration of 2'-MOE mesyl phosphoramidate oligonucleotide does not improve *in vivo* efficacy over 2'-MOE phosphorothioate (nusinersen). The Taiwanese SMA model [52] recapitulates the severe form of SMA through significant weight loss, reduced movement and early onset death between PND7 and PND12. Pups were treated with 20, 30 or 40 μg/g of ISSN1 targeted oligonucleotides MOE-Nus-m and MOE-Nus-s and the respective control oligonucleotides *via* subcutaneous injections on day of birth. We used low doses to distinguish activity between the two ASO chemistries. Weights and survival were monitored daily (Fig. 5). Pups treated with 20, 30, or 40 μg/g MOE-Nus-s survived a median age of 9, 9, and 222 days respectively (Fig. 5, a). The median survival for similarly treated MOE-Nus-m treated pups was 5.5, 15 and 18 days respectively (Fig. 5, b). 40 μg/g MOE-Nus-s survival was statistically significant from untreated ($p < 0.0005$) as well as 40 μg/g MOE-Nus-m treated pups ($p < 0.01$) (Fig. 3, c). Weights between 40 μg/g MOE-Nus-s and control MOE-s treated pups were statistically different ($p < 0.005$)

(Fig. 5, e), however, there was no significant difference in weights at 40 μg/g dose between MOE-Nus-m and MOE-Nus-s (Fig. 5, f).

Discussion

We have recently synthesized novel DNA derivatives incorporating tosyl (*p*-toluenesulfonyl) [54], mesyl (methanesulfonyl) [43] and busyl (1-butanesulfonyl) [45] phosphoramidate groups, respectively, and demonstrated that they can form complementary duplexes with RNA, which were more (tosyl) [54] or less (mesyl or busyl) destabilized [43, 45] in comparison with the native DNA:RNA heteroduplex even if such groups replace all the phosphates in the oligonucleotide chain. In particular, when the least bulky mesyl phosphoramidate (μ) groups were incorporated into an oligodeoxynucleotide sequence, the thermal stabilities of the resulting duplexes with either DNA or RNA showed only slight differences from the corresponding native duplexes [43]. This observation prompted us to investigate mesyl phosphoramidate oligodeoxynucleotides (μ-ODN) substituted at every internucleotidic position with the μ-modification as potential RNase H-recruiting antisense agents targeting pro-oncogenic miRNAs. Our study has confirmed that μ-ODN were able to recruit RNase H mediated miRNA cleavage with similar efficiency to phosphorothioate oligodeoxynucleotides (PS-ODNs) and better than the native DNA [42]. The μ-oligonucleotides were demonstrated to possess nuclease stability in the presence of serum considerably exceeding that of PS-ODNs. Their antisense activity against melanoma B16 cells was also more pronounced and selective and inhibition of miR-21, miR-17 and miR-155 was longer-lasting than in the case of the corresponding PS-ODNs [42]. In addition, G-rich μ-ODNs have been

shown to form parallel G-quadruplexes, which were nearly as stable as the native counterparts [55].

Inspired by these results, we set out to investigate the possibility of a successful design of steric blocking antisense oligonucleotides by substituting 2'-*O*-methylribonucleosides (2'-OMe) or 2'-*O*-(2-methoxyethyl)ribonucleosides (2'-MOE) for 2'-deoxynucleosides in the μ-oligonucleotide backbone. Such a replacement is known to abort any RNase H activation undesirable for a splice-switching application [44]. In addition, we expected that the increase in overall hydrophobicity by introducing busyl (1-butanesulfonyl) phosphoramidate groups (β) [45] may favorably affect cellular uptake of the oligonucleotides.

Activity of ASO 2'deoxyribose and backbone modifications was measured *in vitro* within SMA patient derived fibroblasts. 2'-Deoxyribose ASOs were not effective at inducing splicing modulation. This is to be expected given their RNase H recruitment activity. Both 2'-OMe and 2'-MOE ASOs actively induced splice switching of human *SMN2* exon 7 when paired with the PS or μ internucleotidic linkages. Curiously, the β analogue showed no activity in any ASO. Neither the endosomal escape or intranuclear localization data could explain this observation.

It is commonly believed that ASOs enter cells via a combination of adsorptive, fluid-phase and receptor-mediated endocytosis [56, 57]. This process and intracellular trafficking are accompanied by more than 60 proteins that can bind to ASO and modulate their activity in the cell. Among them are several proteins that compete with RNase H for binding to the heteroduplex formed by PS-ASO with RNA (e.g.,

Ku70, Ku80, P54nrb, and hnRNPs) [58] and can reduce target degradation. Also, binding to proteins affects the subcellular localization of ASO. For example, binding of paraspeckle protein P54nrb or nucleophosmin to ASO increases their accumulation in the nucleus [59, 60]. On average, the increase in hydrophobicity of the 2'-substituent in ASO increased non-specific protein binding [32]. In our study, an increase in hydrophobicity of the ASO either in 2'-deoxy → 2'-OMe → 2'-MOE row, or from mesyl to busyl affected their cellular uptake and intracellular distribution including nuclear localization (Fig. 3 and 4). Whereas both 2'-deoxy phosphorothioate (PS), mesyl and busyl phosphoramidate oligonucleotides demonstrated high level of endosome release (Fig. 3, A), the level of endosomal release of 2'-OMe ASOs was dependent on the backbone modification: phosphorothioate (me Nus-s) demonstrated lower endosomal release (~60%) in comparison with ~83% and ~72% for mesyl (μ) and busyl (β) phosphoramidate oligonucleotides, respectively (Fig. 3, B). However, in the 2'-MOE series, the μ-oligonucleotides showed the lowest endosomal release in comparison with both PS and β-series (Fig. 3, C).

Analysis of the Z-stack microscopy images on the fixed cells after 24 h incubation with Cy5-labeled ASOs demonstrated the accumulation of 2’-deoxy phosphorothioate, 2’-OMe mesyl phosphoramidate ASO and all three variants of 2’-MOE ASO in different compartments of the cell nucleus (Fig. 4).

Differences between expected activity from cellular localization to the nucleus and measured activity may be due to the lipofectamine transfection reagent vs gymnosis uptake. Lipofectamine will aid endosomal escape but not nuclear transport.

Subcutaneous administration to SMA model newborn mice of the 2'-MOE mesyl oligonucleotide isosequential to nusinersen (MOE-Nus-m) even at the highest evaluated dose of 40 mg/kg resulted in a median survival of only 18 days (Fig. 3, a), while the 2'-MOE phosphorothioate (nusinersen) enabled median survival of the pups for 222 days (Fig. 3, b), whereas lower doses of both ASO (20 and 30 mg/kg) were inactive. Observed effect was sequence-specific as the control scrambled and luciferase oligonucleotides did not show any activity (Fig. 3, d, e). However, there were no statistically significant difference in the weights of the pups between nusinersen and its mesyl analog at 40 mg/kg (Fig. 3, f).

These results could possibly be rationalized in the light of confocal microscopy data on cellular uptake and endosomal release of 2'-MOE oligonucleotides with phosphorothioate or mesyl phosphoramidate backbone in the live cells. The release level of 2'-MOE mesyl phosphoramidate oligonucleotides was approximately 2 times less in comparison with 2'-MOE phosphorothioate oligonucleotides. It is suggestive of an issue with endosomal escape for this type of ASO, which may have affected their *in vivo* activity as potential splice-switching agents but, of course, the cellular model we used for uptake studies is not perfect. Furthermore, the differences in biodistribution and metabolism of the phosphorothioate and mesyl phosphoramidate oligonucleotides could be responsible for the disparate in vivo

results similarly to what has been shown recently by direct comparison of the in vivo efficacy of MOE PS (nusinersen) and morpholino phosphordiamidate oligonucleotide (PMO) in a severe mouse SMA model [61]. Thus, additional studies are required to elucidate bioavailability and pharmacokinetics of mesyl phosphoramidate oligonucleotides.

The subtle differences in cytoplasmic and nuclear localization of the 2'-MOE mesyl ON as compared to the 2'-MOE PS ON may reflect different patterns of protein binding and, thus, different pathways of endosomal escape and nuclear uptake for these two phosphate modifications. It may be concluded that protein binding of mesyl phosphoramidates may be less avid than for phosphorothioates and, while it may decrease systemic toxicity as it has been shown recently for RNase H-competent mesyl oligodeoxynucleotides [62], although it is not a serious concern in the case of nusinersen as it is not delivered systemically, it may also affect their antisense activity *in vivo*, particularly when combined with alterations in the pentose sugar from 2-deoxy to 2-MOE-ribose. As the quest for new chemistries for splice switching applications continues to constantly produce yet untried structural combinations [63, 64], it places the present work despite the somewhat discouraging in vivo results, into a wider context of elucidating ‘structure – activity’ patterns for steric block antisense oligonucleotides with altered sugar-phosphate backbone. Thus, alternatives to the common phosphorothioates or PMOs such as mesyl and other sulfonyl phosphoramidate oligonucleotides merit further investigation as potential antisense therapeutics.

To conclude, we have found that the mesyl phosphoramidate oligo-2'-*O*-(2-methoxyethyl) ribonucleotide (2'-MOE μ-ASO) equivalent of nusinersen was not as effective as the FDA-approved 2'-MOE phosphorothioate drug in promoting long-term survival of neonatal mice in the mouse model of spinal muscular atrophy (SMA) even at the highest dose of 40 mg/kg. The low activity of 2'-MOE μ-ASO as compared to nusinersen could be possibly ascribed to less efficient endosomal release and/or nuclear uptake of the 2'-*O*-alkyl RNA oligonucleotides having mesyl (μ) or busyl (β) phosphoramidate internucleotidic linkages as suggested by confocal microscopy study in live HEK293 cells. This may imply different pathways for intracellular trafficking and nuclear import for mesyl phosphoramidate (μ) oligonucleotides with either DNA or 2'-*O*-alkyl RNA backbones. The data obtained may be useful for rational design of antisense oligonucleotides with predominantly cytoplasmic or nuclear mode of action.

Acknowledgements

SMH funding comes from the Medical Research Council (MRC grant No. MR/R025312/1). The SMA mouse model and patient fibroblasts were obtained through an MTA. Microscopy studies were supported by the Institute of Cytology and Genetics (Novosibirsk, Russia) project No. 0324-2019-0042-C-01. TSZ and DAS acknowledge financial support from the Russian Foundation for Basic Research (DAS from grants Nos. 18-515-57006, 18-29-09045 and 18-29-08062, and TSZ from grant No. 19-04-00298).

Author Disclosure Statement

Authors declare no competing financial interests.

References

1. Crooke ST. (2017). Molecular mechanisms of antisense oligonucleotides. Nucleic Acid Ther 27:70-77.
2. Shen X and Corey DR. (2018). Chemistry, mechanism and clinical status of antisense oligonucleotides and duplex RNAs. Nucleic Acids Res 46:1584-1600.
3. Smith CIE, Zain R (2019). Therapeutic Oligonucleotides: State of the Art. Annu Rev Pharmacol Toxicol 59:605-630.
4. Evers MM, Toonen LJA, and van Roon-Mom WMC. (2015). Antisense oligonucleotides in therapy for neurodegenerative disorders. Adv Drug Deliv Rev 87:90-103.
5. Gait MJ, Arzumanov AA, McClorey G, Godfrey C, Betts C, Hammond S, and Wood MJA. (2019) Cell-Penetrating Peptide Conjugates of Steric Blocking Oligonucleotides as Therapeutics for Neuromuscular Diseases from a Historical Perspective to Current Prospects of Treatment. Nucleic Acid Ther 29:1-12.
6. Bennett CF, Baker BF, Pham N, Swayze E, and Geary RS. (2017). Pharmacology of Antisense Drugs. Annu. Rev. Pharmacol. Toxicol. 57:81-105.
7. Castanotto D, Stein CA. (2014). Antisense oligonucleotides in cancer. Curr Opin Oncol 26:584-589.

8. Wagner A, Bock CT, Fechner H, and Kurreck J. (2015). Application of modified antisense oligonucleotides and siRNAs as antiviral drugs. Future Med Chem 7:1637-1642.

9. Hegarty JP and Stewart DB Sr. (2018). Advances in therapeutic bacterial antisense biotechnology. Appl Microbiol Biotechnol. 102:1055-1065.

10. Shimo T, Maruyama R, Yokota T. (2018). Designing Effective Antisense Oligonucleotides for Exon Skipping. Methods Mol Biol. 1687:143-155.

11. Hua Y and Krainer AR. (2012). Antisense-mediated exon inclusion. Methods Mol Biol. 867:307-323.

12. Aartsma-Rus A, Straub V, Hemmings R, Haas M, Schlosser-Weber G, Stoyanova-Beninska V, Mercuri E, Muntoni F, Sepodes B, Vroom E, Balabanov P. (2017). Development of exon skipping therapies for Duchenne Muscular Dystrophy: a critical review and a perspective on the outstanding issues. Nucleic Acid Ther 27:251-259.

13. Hammond SM, Abendroth F, Gait MJ, Wood MJA. (2019). Evaluation of Cell-Penetrating Peptide Delivery of Antisense Oligonucleotides for Therapeutic Efficacy in Spinal Muscular Atrophy. Methods Mol. Biol. 2036:221-236.

14. Aartsma-Rus A, Krieg AM. (2017). FDA Approves Eteplirsen for Duchenne Muscular Dystrophy: The Next Chapter in the Eteplirsen Saga. Nucleic Acid Ther 27:1-3.

15. He YA. (2020). Golodirsen: First Approval. Drugs Feb 6. doi: 10.1007/s40265-020-01267-2. [Epub ahead of print]

16. Aartsma-Rus A. (2017). FDA Approval of Nusinersen for Spinal Muscular Atrophy Makes 2016 the Year of Splice Modulating Oligonucleotides. Nucleic Acid Ther 2:67-69.

17. Lefebvre S, Burglen L, Reboullet S, Clermont O, Burlet P, Viollet L, Benichou B, Cruaud C, Millasseau P, Zeviani M, et al. (1995). Identification and characterization of a spinal muscular atrophy-determining gene. Cell 80:155-165.

18. Wirth B. (2000). An update of the mutation spectrum of the survival motor neuron gene (SMN1) in autosomal recessive spinal muscular atrophy (SMA). Hum Mutat 15:228-237.

19. Cartegni L and Krainer AR. (2002). Disruption of an SF2/ASF-dependent exonic splicing enhancer in SMN2 causes spinal muscular atrophy in the absence of SMN1. Nat Genet 30:377-384.

20. Kashima T and Manley JL. (2003). A negative element in SMN2 exon 7 inhibits splicing in spinal muscular atrophy. Nat Genet 34:460-463.

21. Lorson CL, Hahnen E, Androphy EJ, and Wirth B. (1999). A single nucleotide in the SMN gene regulates splicing and is responsible for spinal muscular atrophy. Proc Natl Acad Sci USA 96:6307-6311.

22. Monani UR, Lorson CL, Parsons DW, Prior TW, Androphy EJ, Burghes AH, and McPherson JD. (1999). A single nucleotide difference that alters splicing

patterns distinguishes the SMA gene SMN1 from the copy gene SMN2. Hum Mol Genet 8:1177-1183.

23. Le TT, Pham LT, Butchbach ME, Zhang HL, Monani UR, Coovert DD, Gavrilina TO, Xing L, Bassell GJ, and Burghes AH. (2005). SMNDelta7, the major product of the centromeric survival motor neuron (SMN2) gene, extends survival in mice with spinal muscular atrophy and associates with full-length SMN. Hum Mol Genet 14:845-857.

24. Hua Y, Vickers TA, Baker BF, Bennett CF, and Krainer AR. (2007). Enhancement of SMN2 exon 7 inclusion by antisense oligonucleotides targeting the exon. PLoS Biol 5:e73.

25. FDA press release on nusinersen approval. https://www.fda.gov/news-events/press-announcements/fda-approves-first-drug-spinal-muscular-atrophy.

26. Singh NK, Singh NN, Androphy EJ, and Singh RN. (2006). Splicing of a critical exon of human Survival Motor Neuron is regulated by a unique silencer element located in the last intron. Mol Cell Biol 26:1333-1346.

27. Finkel, et al. (2017). Nusinersen versus Sham Control in Infantile-Onset Spinal Muscular Atrophy N Engl J Med 377:1723-1732.

28. Stolte B, Totzeck A, Kizina K, Bolz S, Pietruck L, Mönninghoff C, Guberina N, Oldenburg D, Forsting M, Kleinschnitz C, and Hagenacker T. (2018). Feasibility and safety of intrathecal treatment with nusinersen in adult patients

with spinal muscular atrophy. Ther Adv Neurol Disord 11:1756286418803246.

29. Wurster CD, Winter B, Wollinsky K, Ludolph AC, Uzelac Z, Witzel S, Schocke M, Schneider R, and Kocak T. (2019). Intrathecal administration of nusinersen in adolescent and adult SMA type 2 and 3 patients. J Neurol 266:183-194.

30. Eckstein F. (2014). Phosphorothioates, essential components of therapeutic oligonucleotides. Nucleic Acid Ther 24:374-87.

31. Geary RS, Norris D, Yu R, and Bennett CF. (2015). Pharmacokinetics, biodistribution and cell uptake of antisense oligonucleotides. Adv Drug Deliv Rev 87:46-51.

32. Crooke ST, Wang S, Vickers TA, Shen W, and Liang XH. (2017). Cellular uptake and trafficking of antisense oligonucleotides. Nat Biotechnol 35:230-237.

33. Hagedorn PH, Yakimov V, Ottosen S, Kammler S, Nielsen NF, Høg AM, Hedtjärn M, Meldgaard M, Møller MR, Orum H, et al. (2013). Hepatotoxic potential of therapeutic oligonucleotides can be predicted from their sequence and modification pattern. Nucleic Acid Ther 23:302-310.

34. Shen W, De Hoyos CL, Sun H, Vickers TA, Liang XH, and Crooke ST. (2018). Acute hepatotoxicity of 2’ fluoro-modified 5-10-5 gapmer phosphorothioate oligonucleotides in mice correlates with intracellular

protein binding and the loss of DBHS proteins. Nucleic Acids Res 46:2204-2217.

35. Henry SP, Giclas PC, Leeds J, Pangburn M, Auletta C, Levin AA, and Kornbrust DJ. (1997). Activation of the alternative pathway of complement by a phosphorothioate oligonucleotide: Potential mechanism of action. J Pharmacol Exp Ther 281:810-816.

36. Jason TL, Koropatnick J, and Berg RW. (2004). Toxicology of antisense therapeutics. Toxicol Appl Pharmacol 201:66-83.

37. Stein CA and Castanotto D. (2017). FDA-Approved Oligonucleotide Therapies. Mol Ther 25:1069-1075.

38. van Putten M, Tanganyika-de Winter C, Bosgra S, and Aartsma-Rus A. (2019). Nonclinical Exon Skipping Studies with 2'-O-Methyl Phosphorothioate Antisense Oligonucleotides in mdx and mdx-utrn−/− Mice Inspired by Clinical Trial Results. Nucleic Acid Ther 29:92-103.

39. Khvorova A and Watts JK. (2017). The chemical evolution of oligonucleotide therapies of clinical utility. Nat Biotechnol 35:238-248.

40. Shen W, De Hoyos CL, Migawa MT, Vickers TA, Sun H, Low A, Bell TA 3rd, Rahdar M, Mukhopadhyay S, Hart CE, et al. (2019). Chemical modification of PS-ASO therapeutics reduces cellular protein-binding and improves the therapeutic index. Nat Biotechnol 37:640-650.

41. Siva K, Covello G, and Denti MA. (2014). Exon-Skipping Antisense Oligonucleotides to Correct Missplicing in Neurogenetic Diseases. Nucleic Acid Ther 24:69-86.

42. Miroshnichenko SK, Patutina OA, Burakova EA, Chelobanov BP, Fokina AA, Vlassov VV, Altman S, Zenkova MA, and Stetsenko DA. (2019). Mesyl phosphoramidate antisense oligonucleotides as an alternative to phosphorothioates: improved biochemical and biological properties. Proc Natl Acad Sci USA 116:1229-1234.

43. Burakova EA, Derzhalova AS, Chelobanova BP, Fokina AA, and Stetsenko DA. (2019). New Oligodeoxynucleotide Derivatives Containing *N*-(Sulfonyl)-Phosphoramide Groups. Russ J Bioorg Chem 45:662-668.

44. Lima WF and Crooke ST. (1997). Binding affinity and specificity of Escherichia coli RNase H1: impact on the kinetics of catalysis of antisense oligonucleotide-RNA hybrids. Biochemistry 36:390-398.

45. Chelobanov BP, Burakova EA, Prokhorova DV, Fokina AA, and Stetsenko DA. (2017). New oligodeoxynucleotide derivatives containing *N*-(methanesulfonyl)-phosphoramidate (mesyl phosphoramidate) internucleotide group. Russ J Bioorg Chem 43:664-668.

46. Farzan VM, Ulashchik EA, Martynenko-Makaev YV, Kvach MV, Aparin IO, Brylev VA, Prikazchikova TA, Maklakova SY, Majouga AG, Ustinov AV, Shipulin GA, Shmanai VV, Korshun VA, Zatsepin TS. (2017). Automated Solid-Phase Click Synthesis of Oligonucleotide Conjugates: From Small

Molecules to Diverse *N*-Acetylgalactosamine Clusters. Bioconjug Chem 28:2599-2607.

47. Honcharenko M, Honcharenko D, Strömberg R. (2019). Efficient Conjugation to Phosphorothioate Oligonucleotides by Cu-Catalyzed Huisgen 1,3-Dipolar Cycloaddition. Bioconjug Chem 30:1622-1628.

48. Hammond SM, Abendroth F, Gait MJ, Wood MJA. (2019). Evaluation of Cell-Penetrating Peptide Delivery of Antisense Oligonucleotides for Therapeutic Efficacy in Spinal Muscular Atrophy. Methods Mol Biol (Clifton, N.J.) 2036: 221-236.

49. Ramakers C, Ruijter JM, Lekanne Deprez RH, Moorman AFM. (2003). Assumption-free analysis of quantitative real-time polymerase chain reaction (PCR) data. Neurosci Lett 339:62-66.

50. Ruijter JM, Ramakers C, Hoogaars WMH, Karlen Y, Bakker O, van den Hoff MJB, Moorman AFM. (2009). Amplification efficiency: linking baseline and bias in the analysis of quantitative PCR data. Nucleic Acids Res 37:e45.

51. Pfaffl MW. (2001). A New Mathematical Model for Relative Quantification in Real-Time RT-PCR. Nucleic Acid Res 29:e45.

52. Hsieh-Li HM, et al. (2000). A mouse model for spinal muscular atrophy. Nat Genet 24:66-70.

53. Gogliotti RG, Hammond SM, Lutz C, and DiDonato CJ. (2010). Molecular and phenotypic reassessment of an infrequently used mouse model for spinal muscular atrophy. Biochem Biophys Res Commun 391:517.

54. Prokhorova DV, Chelobanov BP, Burakova EA, Fokina AA, and Stetsenko DA. (2017). New Oligodeoxyribonucleotide Derivatives Bearing Internucleotide *N*-Tosyl Phosphoramidate Groups: Synthesis and Complementary Binding to DNA and RNA. Russ J Bioorg Chem 43:38-42.

55. Su Y, Fujii H, Burakova EA, Chelobanov BP, Fujii M, Stetsenko DA, and Filichev VV. (2019). Neutral and Negatively Charged Phosphate Modifications Altering Thermal Stability, Kinetics of Formation and Monovalent Ion Dependence of DNA G-Quadruplexes. Chem Asian J 14:1212-1220.

56. Akhtar S, Juliano RL. (1992). Cellular uptake and intracellular fate of antisense oligonucleotides. Trends Cell Biol 2:139-144.

57. Juliano RL, Carver K, Cao C, Ming X. (2013). Receptors, endocytosis, and trafficking: the biological basis of targeted delivery of antisense and siRNA oligonucleotides. J Drug Target 21:27-43.

58. Liang XH, Shen W, Sun H, Kinberger GA, Prakash TP, Nichols JG, Crooke ST. (2016). Hsp90 protein interacts with phosphorothioate oligonucleotides containing hydrophobic 2'-modifications and enhances antisense activity. Nucleic Acids Res 44:3892-3907.

59. Liang XH, Sun H, Shen W, Crooke ST. (2015). Identification and characterization of intracellular proteins that bind oligonucleotides with phosphorothioate linkages. Nucleic Acids Res 43:2927-2945.

60. Shen W, Liang XH, Sun H, Crooke ST. (2015). 2’-Fluoro-modified phosphorothioate oligonucleotide can cause rapid degradation of P54nrb and PSF. Nucleic Acids Res 43:4569-4578.

61. Sheng L, Rigo F, Bennett CF, Krainer AR, Hua Y. (2020) Comparison of the efficacy of MOE and PMO modifications of systemic antisense oligonucleotides in a severe SMA mouse model. Nucleic Acids Res 48:2853-2865.

62. Patutina OA, Gaponova (Miroshnichenko) SK, Sen’kova AV, Savin IA, Gladkikh DV, Burakova EA, Fokina AA, Maslov MA,. Shmendel’ EV, Wood MJA, Vlassov VV, Altman S, Stetsenko DA, Zenkova MZ. (2020) Mesyl phosphoramidate backbone modified antisense oligonucleotides targeting miR-21 with enhanced in vivo therapeutic potency. Proc Natl Acad Sci USA 117:32370-32379.

63. Le BT, Adams AM, Fletcher S, Wilton SD, Veedu RN. (2017). Rational Design of Short Locked Nucleic Acid-Modified 2’-O-Methyl Antisense Oligonucleotides for Efficient Exon-Skipping in Vitro. Mol Ther Nucleic Acids 9:155-161.

64. Hande M, Saher O, Lundin KE, Smith CIE, Zain R, Lönnberg T. (2019). Oligonucleotide-Palladacycle Conjugates as Splice-Correcting Agents. Molecules 24: E1180.

Tables

Table 1. Sequences and molecular masses of modified oligonucleotides.

Name	Sequence, 5'-3'	Molecular mass[a], Da	
		Calcd.	Exper.
dNus-S	d(T$_S$[b]C$_S$A$_S$C$_S$T$_S$T$_S$T$_S$C$_S$A$_S$T$_S$A$_S$A$_S$T$_S$G$_S$C$_S$T$_S$G$_S$G$_S$)	5933.0	5937.3
	d(T$_S$[b]C$_S$A$_S$C$_S$T$_S$T$_S$T$_S$C$_S$A$_S$T$_S$A$_S$A$_S$T$_S$G$_S$C$_S$T$_S$G$_S$G$_S$)-Cy5[c]	6558.0	6563.8
dNus-m	d(T$^{\mu}$[d]C$^{\mu}$A$^{\mu}$C$^{\mu}$T$^{\mu}$T$^{\mu}$T$^{\mu}$C$^{\mu}$A$^{\mu}$T$^{\mu}$A$^{\mu}$A$^{\mu}$T$^{\mu}$G$^{\mu}$C$^{\mu}$T$^{\mu}$G$^{\mu}$G$^{\mu}$)	7123.8	7127.1
	d(T$^{\mu}$[d]C$^{\mu}$A$^{\mu}$C$^{\mu}$T$^{\mu}$T$^{\mu}$T$^{\mu}$C$^{\mu}$A$^{\mu}$T$^{\mu}$A$^{\mu}$A$^{\mu}$T$^{\mu}$G$^{\mu}$C$^{\mu}$T$^{\mu}$G$^{\mu}$G$^{\mu}$)-Cy5	7947.7	7856.1
dNus-bm	d(T$^{\beta}$[e]C$^{\beta}$A$^{\beta}$C$^{\beta}$T$^{\beta}$T$^{\beta}$T$^{\beta}$C$^{\beta}$A$^{\beta}$T$^{\beta}$A$^{\beta}$A$^{\beta}$T$^{\beta}$G$^{\beta}$C$^{\beta}$T$^{\beta}$G$^{\beta}$G$^{\beta}$)	7879.8	7882.0
	d(T$^{\beta}$[e]C$^{\beta}$A$^{\beta}$C$^{\beta}$T$^{\beta}$T$^{\beta}$T$^{\beta}$C$^{\beta}$A$^{\beta}$T$^{\beta}$A$^{\beta}$A$^{\beta}$T$^{\beta}$G$^{\beta}$C$^{\beta}$T$^{\beta}$G$^{\beta}$G$^{\beta}$)-Cy5	8603.0	8611.1
me-Nus-S	2'-OMe-r(U$_S$C$_S$A$_S$C$_S$U$_S$U$_S$U$_S$C$_S$A$_S$U$_S$A$_S$A$_S$U$_S$G$_S$C$_S$U$_S$G$_S$G$_S$)	6375.2	6380.2
	2'-OMe-r(U$_S$C$_S$A$_S$C$_S$U$_S$U$_S$U$_S$C$_S$A$_S$U$_S$A$_S$A$_S$U$_S$G$_S$C$_S$U$_S$G$_S$G$_S$)-Cy5	7000.2	7002.2
me-Nus-m	2'-OMe-r(U$^{\mu}$C$^{\mu}$A$^{\mu}$C$^{\mu}$U$^{\mu}$U$^{\mu}$U$^{\mu}$C$^{\mu}$A$^{\mu}$U$^{\mu}$A$^{\mu}$A$^{\mu}$U$^{\mu}$G$^{\mu}$C$^{\mu}$U$^{\mu}$G$^{\mu}$G$^{\mu}$)	7566.1	7571.2
	2'-OMe-r(U$^{\mu}$C$^{\mu}$A$^{\mu}$C$^{\mu}$U$^{\mu}$U$^{\mu}$U$^{\mu}$C$^{\mu}$A$^{\mu}$U$^{\mu}$A$^{\mu}$A$^{\mu}$U$^{\mu}$G$^{\mu}$C$^{\mu}$U$^{\mu}$G$^{\mu}$G$^{\mu}$)-Cy5	8290.0	8296.9
me-Nus-bm	2'-OMe-r(U$^{\beta}$C$^{\beta}$A$^{\beta}$C$^{\beta}$U$^{\beta}$U$^{\beta}$U$^{\beta}$C$^{\beta}$A$^{\beta}$U$^{\beta}$A$^{\beta}$A$^{\beta}$U$^{\beta}$G$^{\beta}$C$^{\beta}$U$^{\beta}$G$^{\beta}$G$^{\beta}$)	8322.1	8325.0
	2'-OMe-r(U$^{\beta}$C$^{\beta}$A$^{\beta}$C$^{\beta}$U$^{\beta}$U$^{\beta}$U$^{\beta}$C$^{\beta}$A$^{\beta}$U$^{\beta}$A$^{\beta}$A$^{\beta}$U$^{\beta}$G$^{\beta}$C$^{\beta}$U$^{\beta}$G$^{\beta}$G$^{\beta}$)-Cy5	9046.0	9051.2
MOE-Nus-s	2'-MOE-r(T$_S$C^m$_S$A$_S$C^m$_S$T$_S$T$_S$T$_S$C^m$_S$A$_S$T$_S$A$_S$A$_S$T$_S$G$_S$C^m$_S$T$_S$G$_S$G$_S$)	7317.3	7323.2
	2'-MOE-r(T$_S$C^m$_S$A$_S$C^m$_S$T$_S$T$_S$T$_S$C^m$_S$A$_S$T$_S$A$_S$A$_S$T$_S$G$_S$C^m$_S$T$_S$G$_S$G$_S$)-Cy5	7942.3	7948.6
MOE-Nus-m	2'-MOE-r(T$^{\mu}$C$^{m\mu}$A$^{\mu}$C$^{m\mu}$T$^{\mu}$T$^{\mu}$T$^{\mu}$C$^{m\mu}$A$^{\mu}$T$^{\mu}$A$^{\mu}$A$^{\mu}$T$^{\mu}$G$^{\mu}$C$^{m\mu}$T$^{\mu}$G$^{\mu}$G$^{\mu}$)	8509.0	8517.9
	2'-MOE-r(T$^{\mu}$C$^{m\mu}$A$^{\mu}$C$^{m\mu}$T$^{\mu}$T$^{\mu}$T$^{\mu}$C$^{m\mu}$A$^{\mu}$T$^{\mu}$A$^{\mu}$A$^{\mu}$T$^{\mu}$G$^{\mu}$C$^{m\mu}$T$^{\mu}$G$^{\mu}$G$^{\mu}$)-Cy5	9100.0	9108.5
MOE-Nus-bm	2'-MOE-r(T$^{\beta}$C$^{m\beta}$A$^{\beta}$C$^{m\beta}$T$^{\beta}$T$^{\beta}$T$^{\beta}$C$^{m\beta}$A$^{\beta}$T$^{\beta}$A$^{\beta}$A$^{\beta}$T$^{\beta}$G$^{\beta}$C$^{m\beta}$T$^{\beta}$G$^{\beta}$G$^{\beta}$)	9265.0	9271.1
	2'-MOE-r(T$^{\beta}$C$^{m\beta}$A$^{\beta}$C$^{m\beta}$T$^{\beta}$T$^{\beta}$T$^{\beta}$C$^{m\beta}$A$^{\beta}$T$^{\beta}$A$^{\beta}$A$^{\beta}$T$^{\beta}$G$^{\beta}$C$^{m\beta}$T$^{\beta}$G$^{\beta}$G$^{\beta}$)-Cy5	9856.7	9863.0

[a] Conditions of ESI-MS: see Supporting information; [b] (s) – phosphorothioate group; [c] Cy5 fluorescent label; [d] ($^{\mu}$) – mesyl (methanesulfonyl) phosphoramidate group; [e] ($^{\beta}$) – busyl (1-butanesulfonyl) phosphoramidate group; [f] C^m – 5-Me-C residue.

Figures

<Fig. 1>

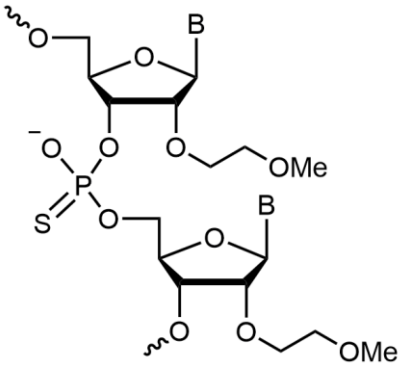

1

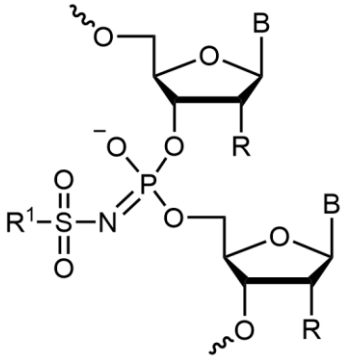

2a R = H, R^1 = Me
2b R = OMe, R^1 = Me
2c R = $O(CH_2)_2OMe$, R^1 = Me
2d R = H, R^1 = *n*-C_4H_9
2e R = OMe, R^1 = *n*-C_4H_9
2f R = $O(CH_2)_2OMe$, R^1 = *n*-C_4H_9

<Fig. 2>

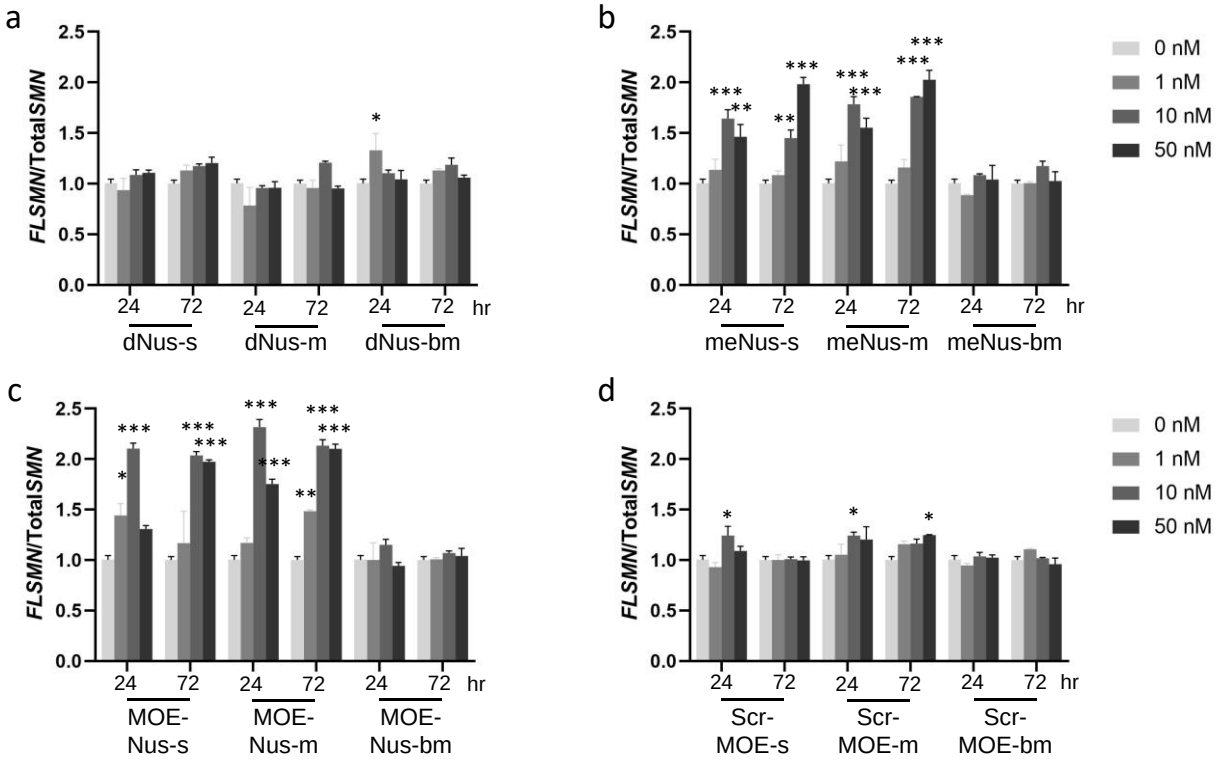

<Fig. 3>

A)

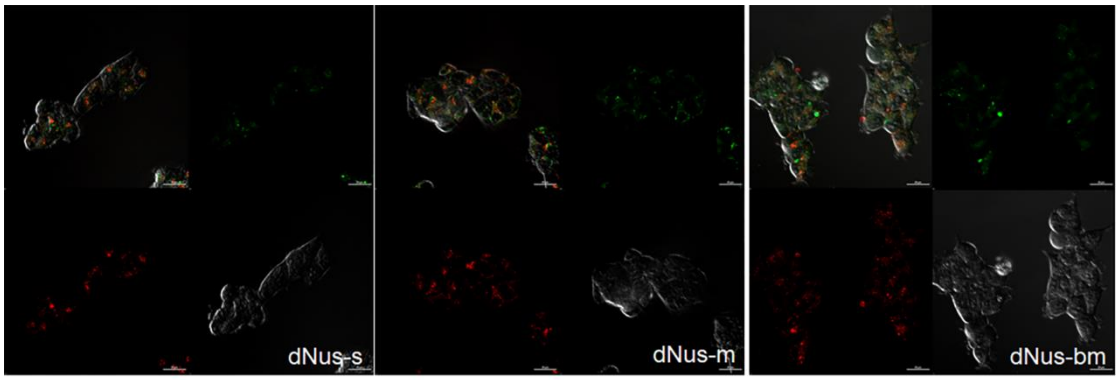
dNus-s
dNus-m
dNus-bm

B)

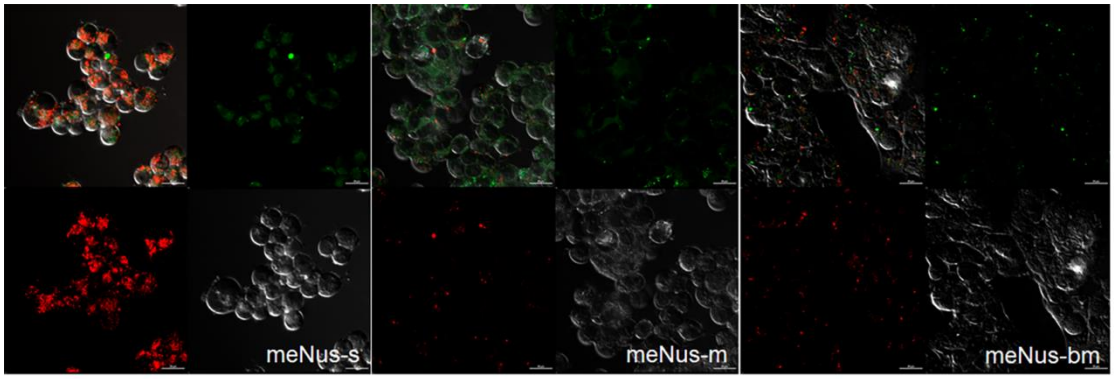
meNus-s
meNus-m
meNus-bm

C)

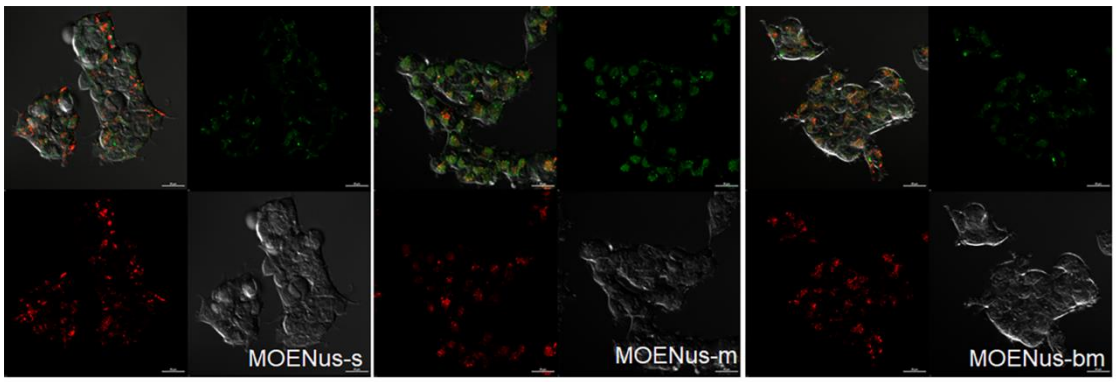
MOENus-s
MOENus-m
MOENus-bm

<Fig. 4>

A)

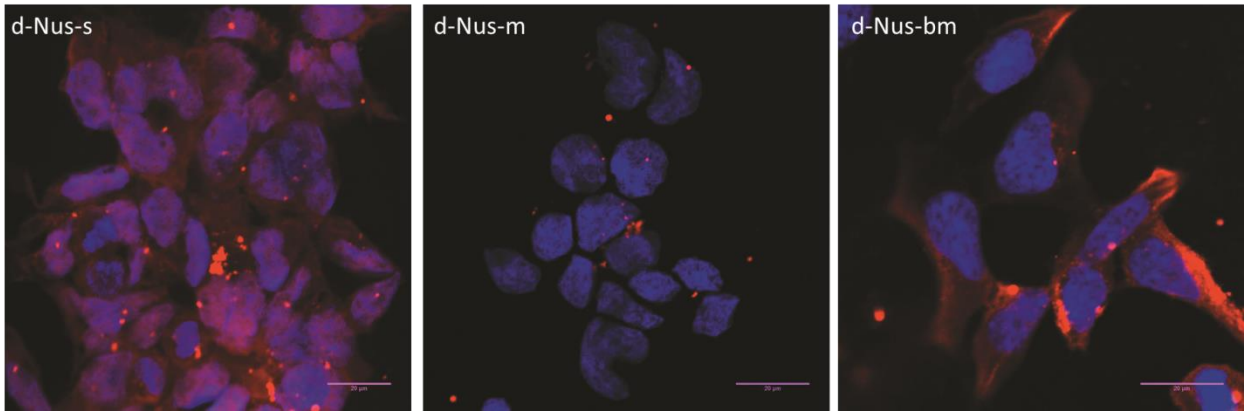
d-Nus-s
d-Nus-m
d-Nus-bm

B)

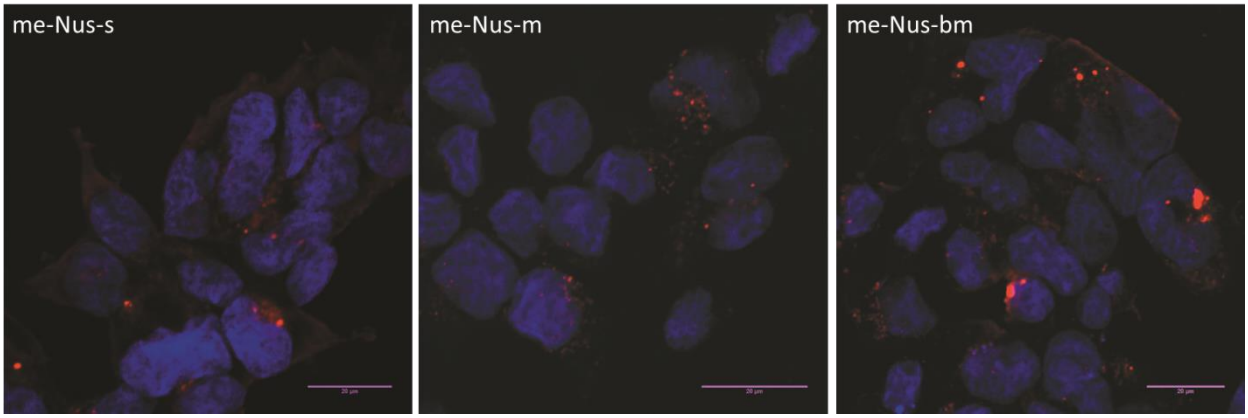
me-Nus-s
me-Nus-m
me-Nus-bm

C)

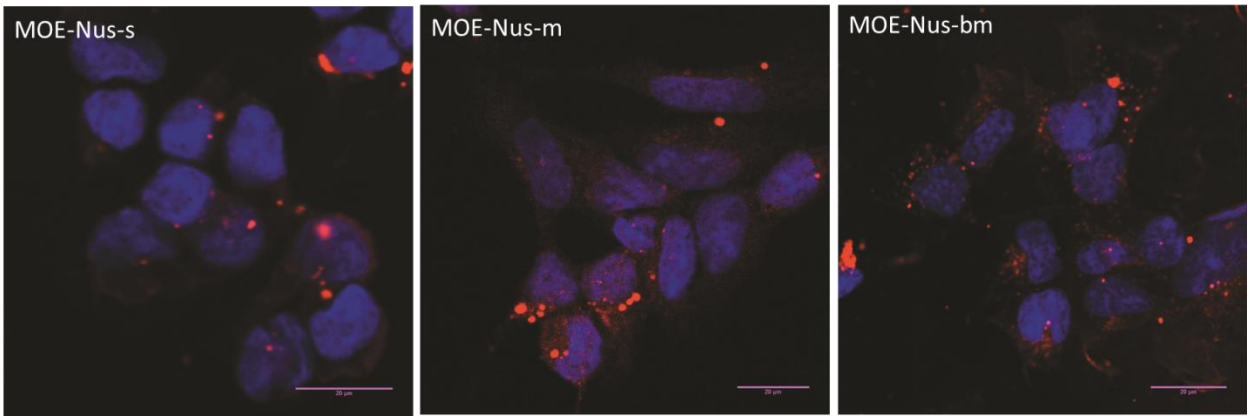
MOE-Nus-s
MOE-Nus-m
MOE-Nus-bm

<Fig. 5>

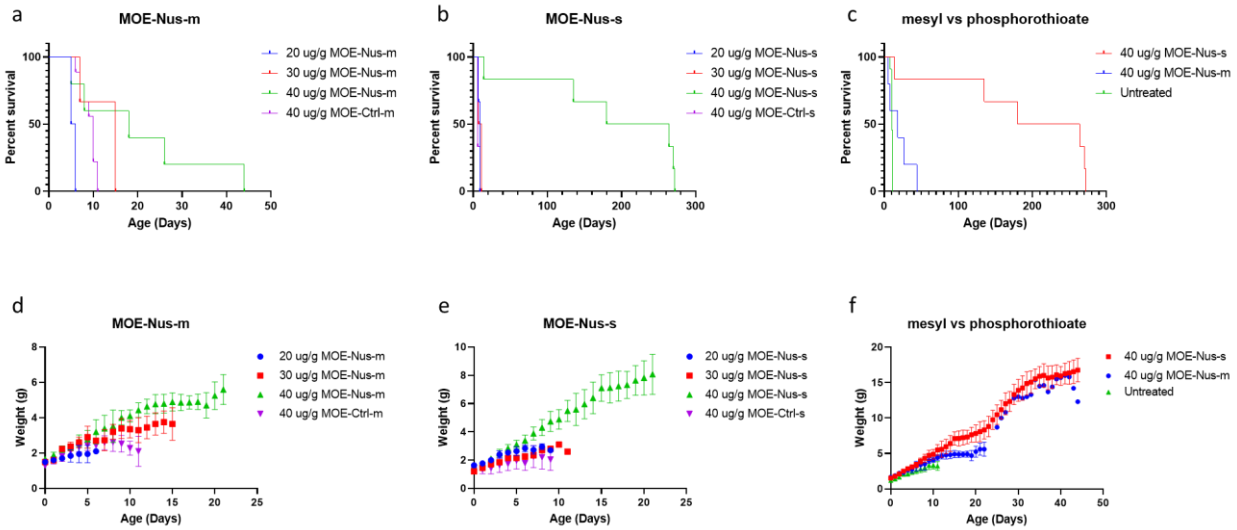
a
MOE-Nus-m
Percent survival
Age (Days)
20 ug/g MOE-Nus-m
30 ug/g MOE-Nus-m
40 ug/g MOE-Nus-m
40 ug/g MOE-Ctrl-m
b
MOE-Nus-s
Percent survival
Age (Days)
20 ug/g MOE-Nus-s
30 ug/g MOE-Nus-s
40 ug/g MOE-Nus-s
40 ug/g MOE-Ctrl-s
c
mesyl vs phosphorothioate
Percent survival
Age (Days)
40 ug/g MOE-Nus-s
40 ug/g MOE-Nus-m
Untreated
d
MOE-Nus-m
Weight (g)
Age (Days)
20 ug/g MOE-Nus-m
30 ug/g MOE-Nus-m
40 ug/g MOE-Nus-m
40 ug/g MOE-Ctrl-m
e
MOE-Nus-s
Weight (g)
Age (Days)
20 ug/g MOE-Nus-s
30 ug/g MOE-Nus-s
40 ug/g MOE-Nus-s
40 ug/g MOE-Ctrl-s
f
mesyl vs phosphorothioate
Weight (g)
Age (Days)
40 ug/g MOE-Nus-s
40 ug/g MOE-Nus-m
Untreated

Figure Legends

Fig. 1. Backbones for splice-switching oligonucleotides (SSOs): oligo-2'-*O*-(2-methoxyethyl)-ribonucleotide phosphorothioate (2'-MOE PS) (**1**) (as in nusinersen); mesyl (methanesulfonyl) phosphoramidate (μ): 2'-deoxy (**2a**), 2'-*O*-methyl (**2b**), and 2'-*O*-(2-methoxyethyl) (2'-MOE) (**2c**); and busyl (1-butanesulfonyl) phosphoramidate (β): 2'-deoxy (**2d**), 2'-*O*-methyl (**2e**), and 2'-*O*-(2-methoxyethyl) (2'-MOE) (**2f**).

Fig. 2. Splice switching activity of ASOs in SMA patient fibroblasts. Cells were treated with 0, 1, 10 or 50 nM ASOs via lipofectamine transfection agent. Splice switching activity was analysed via qPCR (mean ± S.E.M.). ASO chemistries (A) 2'deoxy (d), (B) 2'-OMe (me), and (C) 2'-MOE were tested at 24 and 72 h post-transfection modified with phosphate derivatives phosporothioate (s), mesyl (m) or busyl (bm). (D) Scrambled ASO MOE sequence was used as a control. * P<0.01, ** p<0.001, *** P<0.0001, 2-Way ANOVA with Bonferroni's multiple comparisons test, 99.90% confidence level of difference

Fig. 3. Confocal microscopy images of ASO internalization after 60 min in live HEK293 cells with labeled lysosomes. Panels: A) 2'-deoxy (d-), B) 2'-OMe (me-), and C) 2'-MOE backbone, respectively; Nus-s – phosphorothioate, Nus-m – mesyl (μ), and Nus-bm – busyl (β) phosphoramidate modification, respectively. The Cy5-

labeled antisense oligonucleotide is displayed as red fluorescence, lysosomes are labeled as green fluorescence.

Fig. 4. Confocal microscopy images (z-stacks) of ASO internalization after 24 hours in fixed HEK293 cells. Panels: A) 2'-deoxy (d-), B) 2'-OMe (me-), and C) 2'-MOE backbone, respectively; Nus-s – phosphorothioate, Nus-m – mesyl, and Nus-bm – busyl phosphoramidate modification, respectively. Cy5-labeled ASO are in red, DAPI-stained cell nuclei are in blue.

Fig. 5. Survival and weights in SMA mice treated at PND0. (a) Survival curves for SMA mice treated with 20 (n = 2), 30 (n = 3) or 40 μg/g (n = 5) MOE-Nus-m or 40 μg/g control MOE-m (n = 9). 40 μg/g enhanced survival (mean of 20.2 + 15.7, median of 18 days) but was not statistically significant from untreated pups (mean of 10.3 ± 0.9, median of 10 days). The longest living SMA mouse treated with 40 μg/g MOE-Nus-m survived to 44 days of age. (b) Survival curves for SMA mice treated with 20 (n = 3), 30 (n=2) or 40 μg/g (n = 6) MOE-Nus-s or 40 μg/g control MOE-s (n = 6). (c) 40 μg/g MOE-Nus-s enhanced survival (mean of 189.2 ± 102.7, median of 222 days) and was statistically significant from untreated pups (P = 0.0003) and MOE-Nus-m treated pups (P = 0.0085, log-rank Mantel-Cox test). (d) Weights of pups treated with MOE-Nus-m plotted as mean ± SD. There was no significant difference between treatment groups. (e) Weights of pups treated with MOE-Nus-s up till weaning. Pups treated at 40 μg/g weighted significantly more

than 40 μg/g control treated pups up to PND10 ($P < 0.005$) but not 20 and 30 μg/g treated pups. (f) Direct comparison between MOE-Nus-s and MOE-Nus-m treated pups reveals no significant difference at any age.